

Ocean dynamics determine the response of oceanic CO₂ uptake to climate change

T. Crueger · E. Roeckner · T. Raddatz ·
R. Schnur · P. Wetzel

Received: 18 December 2006 / Accepted: 5 November 2007
© The Author(s) 2007

Abstract The increase of atmospheric CO₂ concentrations due to anthropogenic activities is substantially damped by the ocean, whose CO₂ uptake is determined by the state of the ocean, which in turn is influenced by climate change. We investigate the mechanisms of the ocean's carbon uptake within the feedback loop of atmospheric CO₂ concentration, climate change and atmosphere/ocean CO₂ flux. We evaluate two transient simulations from 1860 until 2100, performed with a version of the Max Planck Institute Earth System Model (MPI-ESM) with the carbon cycle included. In both experiments observed anthropogenic CO₂ emissions were prescribed until 2000, followed by the emissions according to the IPCC Scenario A2. In one simulation the radiative forcing of changing atmospheric CO₂ is taken into account (coupled), in the other it is suppressed (uncoupled). In both simulations, the oceanic carbon uptake increases from 1 GT C/year in 1960 to 4.5 GT C/year in 2070. Afterwards, this trend weakens in the coupled simulation, leading to a reduced uptake rate of 10% in 2100 compared to the uncoupled simulation. This includes a partial offset due to higher atmospheric CO₂ concentrations in the coupled simulation owing to reduced carbon uptake by the terrestrial biosphere. The difference of the oceanic carbon uptake between both simulations is primarily due to partial pressure difference and secondary to solubility changes. These contributions are widely offset by changes of gas transfer velocity due to sea ice melting and wind changes. The major differences appear in the Southern

Ocean (−45%) and in the North Atlantic (−30%), related to reduced vertical mixing and North Atlantic meridional overturning circulation, respectively. In the polar areas, sea ice melting induces additional CO₂ uptake (+20%).

Keywords Ocean carbon cycle · Climate change · Ocean circulation · Climate scenarios · Air–sea CO₂ flux

1 Introduction

The increase of the global temperature during the last 150 years can at least partially be attributed to the increase of atmospheric CO₂ concentrations as a consequence of anthropogenic activities such as the continuous enhancement of fossil fuel burning and deforestation (Houghton et al. 2001). These emissions have led to an increase of atmospheric CO₂ concentrations from 280 ppm in 1800 (Enting et al. 1994) to 369 ppm in 2000 (Keeling and Whorf 2005). This increase, however, accounts only for a portion of the total CO₂ emissions, since only about half of the emissions have been stored in the atmosphere. The ocean takes up more than one third of the released CO₂ (Sarmiento and Gruber 2002; Houghton et al. 2001). Much effort has been made to assess the ocean carbon cycle, especially the budget and spatial distributions of the atmosphere/ocean CO₂ fluxes (Key et al. 2004; Sabine et al. 2004; McNeil et al. 2003; Takahashi et al. 2002; Murnane et al. 1999). Furthermore, simulations with coupled atmosphere ocean general circulation models (AOGCM) with different complexities have been performed to assess the future CO₂ uptake of the oceans under the assumption of continuously increasing CO₂ emissions and the accompanying climate change. Firstly, these simulations did not allow estimating the response of

T. Crueger (✉) · E. Roeckner · T. Raddatz · R. Schnur ·
P. Wetzel
Max Planck Institute for Meteorology,
Bundesstrasse 53, 20146 Hamburg, Germany
e-mail: traute.crueger@zmaw.de

atmospheric CO₂ content to changing CO₂ uptake of the land and the ocean. More recently, such simulations with a full coupling between climate and the carbon cycle have been performed in order to assess the magnitude and the mechanisms of the climate-carbon cycle feedback (Gregory et al. 2005; Dufresne et al. 2002; Friedlingstein et al. 2001, 2003, 2006; Sarmiento et al. 1998; Cao and Woodward 1998).

In a pioneering study, Cox et al. (2000) found a strong positive feedback. Towards the end of the twenty-first century, the atmospheric CO₂ concentration additionally increased by around 250 ppm as a consequence of lesser uptake by both, the land and the ocean, in the warmer climate scenario. Friedlingstein et al. (2003, 2006) investigated the feedback of 11 coupled climate-carbon cycle models. They showed that the feedback between climate change and atmospheric CO₂ is positive. For all models, the climate change-induced atmosphere–land fluxes account for the main contributions, whereas the oceanic contributions are smaller. For all but one models a smaller ocean uptake is found in the simulation including climate warming than in the simulation that suppresses climate warming. This tends to increase atmospheric CO₂ and thus represents a positive feedback contribution of the ocean.

Some potential physical and biogeochemical drivers of the ocean carbon cycle in a warm climate have been discussed earlier, mostly favoring a decrease of oceanic CO₂ uptake due to climate change (Sarmiento et al. 1998, 2004, Sarmiento and Hughes 1999; Plattner et al. 2001; Friedlingstein et al. 2001; Cox et al. 2000; Mignone et al. 2006; Russell et al. 2006):

1. Warming of the ocean decreases the solubility of CO₂ and subsequently the CO₂ uptake by the oceans (reduced solubility pump).
2. Increasing sea surface temperatures and enhanced freshening of the surface water strengthen the thermal stratification. On the one hand this is expected to shallow the mixed layer depth (MLD), leading to less vertical transport of carbon into the deep ocean. On the other hand, the reduced ventilation favors a reduction of nutrient transport to the surface layers and hence primary production in surface waters.
3. Under climate change conditions, the ocean circulation undergoes some significant changes, e.g. a weakening of the Atlantic Meridional Overturning Circulation (Stouffer et al. 2006), which is suggested to reduce the vertical transport of carbon into deep ocean layers.
4. An enhancement and a poleward shift of the main wind belt in the Southern Hemisphere, which are expected in a warmer climate (Bengtsson et al. 2006; Kushner et al. 2001; Yin 2005), are suspected to maintain a robust Southern Ocean Overturning, allowing the

ocean to increase the transport of anthropogenic CO₂ into the deep ocean.

The main scope of this study is to investigate the mechanisms responsible for the projected changes in CO₂ uptake by the oceans. For that reason we evaluate two transient simulations of the Max Planck Institute Earth System Model (MPI-ESM), consisting of the atmosphere, the ocean including the biogeochemistry and the land surface including the vegetation. Both simulations are forced with increasing CO₂ emissions. In both simulations, the atmospheric CO₂ interacts with the terrestrial and oceanic carbon cycle. However, greenhouse gas warming due to increased atmospheric CO₂ is only allowed in one simulation, whereas it is inhibited in the other simulation. Therefore, the differences between CO₂ fluxes reflect the effect of greenhouse gas warming on the carbon cycle. An evaluation of both simulations, with a special focus on the land biosphere, is found in Raddatz et al. (2007). Their study confirms previous findings of a positive climate-carbon cycle feedback. In particular, it is found that this feedback is dominated by the tropical land biosphere, which accounts for more than 80% of the climate change effect, whereas a smaller contribution (<20%) is ascribed to the ocean (Friedlingstein et al. 2006). These simulations were also included in the model intercomparison study of Friedlingstein et al. (2006), who found that the additional atmospheric concentration due to global warming simulated by the MPI-ESM of about 80 ppm in 2100 is within the range of 50–100 ppm obtained for most models. Furthermore they found that the change in CO₂ uptake by both the land and the ocean in the MPI-ESM simulations is also within the range of most models. Although smaller than the contribution of the land, possibly simply due to its lagged response, the ocean carbon-climate feedback is of fundamental interest, since the ocean represents a dominant sink of anthropogenic carbon. Changes of key features of the ocean's carbon cycle, e.g. SST, circulation, sea ice coverage and export, are supposed to modify the ocean carbon cycle, which in turn may lead to fundamental changes of atmospheric CO₂ and hence climate.

In this study, we firstly investigate the global and regional budgets of the CO₂ fluxes and their differences between the coupled and the uncoupled simulation, respectively. Then we examine the processes, which lead to changing CO₂ fluxes due to climate change. For that reason we investigate the properties that determine the atmosphere/ocean CO₂ flux and the atmospheric and oceanic properties relevant for the atmosphere/ocean CO₂ flux. This includes an exploitation of some ocean interior circulation features in those areas, which show a strong CO₂ flux response to climate change.

The paper is structured as follows: an introduction of the model and the experimental setup is given in Sect. 2. In Sect. 3 the applied methodology of this study is described, including a brief introduction of the main parameters determining the atmosphere/ocean CO₂ fluxes. The result Sect. 4 includes the CO₂ fluxes of the two simulations and the changes of atmospheric/oceanic properties relevant for CO₂ fluxes. The associated processes leading to CO₂ flux changes under global warming are discussed in Sect. 5. The conclusions are given in Sect. 6.

2 Model and experimental setup

The simulations were performed with a version of the MPI-ESM. The atmospheric general circulation model is ECHAM5 (Roeckner et al. 2003) employed at T63 horizontal resolution with 31 vertical levels, corresponding to about 1.9° in longitude and latitude. ECHAM5 is coupled to the ocean general circulation model MPI-OM (Marsland et al. 2003). The ocean model employs the primitive equations for a hydrostatic Boussinesq fluid with a free surface at a resolution of 1.5°. The vertical discretization is on 40 z-levels, and the bottom topography is resolved by means of partial grid cells. The poles of the curvilinear grid are shifted to land areas over Greenland and Antarctica. The information between the atmosphere and the ocean is exchanged once per simulated day using the OASIS coupler (Valcke et al. 2003). An evaluation of the key oceanic features simulated by the coupled model can be found in Jungclaus et al. (2006). The ocean model includes the module HAMOCC5.1 for the marine biogeochemistry (Maier-Reimer et al. 2005). This module simulates photosynthesis and zooplankton grazing in the euphotic layer, depending on the nutrients nitrate, phosphate, silicate and iron. The iron is deposited by dust on the water surface. Furthermore, denitrification, N-fixation, DMS production and the formation of calcium carbonate and opaline shells are included. The export of detritus out of the euphotic zone results from the death of phyto- and zooplankton as well as faecal pellets. Below the euphotic layer mortality is described by constant rates of 10% 1/day for phytoplankton and 2% 1/day for zooplankton. In case of sufficient oxygen, aerobic remineralization of dissolved organic matter (DOM) and detritus occur with rates of 3% 1/day and 2.5% 1/day, respectively. A sediment module following Heinze et al. (2003) is also included, describing changes due to non-mineralized particulate matter. As initial conditions, a uniform distribution of the biogeochemical tracers are prescribed, only specifying e.g. the total amount of dissolved inorganic carbon (DIC, 38.000 Gt). The dust fields are taken from a model simulation by Timmreck and Schulz (2004). The capability of the ocean model to simulate a

realistic ocean carbon cycle and air–sea exchange of CO₂ has been assessed by Wetzel et al. (2005) in a simulation forced by daily NCEP/NCAR Reanalysis data.

The terrestrial carbon cycle is simulated by the land surface scheme JSBACH. This is based on the Biosphere Energy Transfer and Hydrology scheme (BETHY, Knorr 2000), which includes photosynthesis for C3 and C4 plants, depending on atmospheric CO₂ concentration. Furthermore, stomatal conductance and heterotrophic respiration are included. Further details of JSBACH and the spin up of the simulations can be found in Raddatz et al. (2007). In our coupled model, the three-dimensional transport of carbon within the ocean and the atmosphere as well as the exchange with the land biosphere are calculated at each model time step (72 min), so that the daily and the seasonal cycles of the atmospheric CO₂ concentration are represented. The carbon flux between the ocean and the atmosphere is determined once per day. In the 150-year control simulation the drift of atmospheric CO₂ was less than 1 ppm, the drift of oceanic DIC less than 2‰. Thus, no flux corrections were performed in the simulations. In order to separate the effects of increasing atmospheric CO₂ and greenhouse gas warming on the vegetation and ocean we performed two transient simulations. The simulations started from a pre-industrial equilibrium, which had been achieved by a 1500-year off-line ocean model simulation followed by a 150-year coupled ocean/atmosphere simulation. The two transient simulations were conducted by adding anthropogenic CO₂ emissions to the lowest layer of the atmosphere as the only forcing: following Marland et al. (2003) for fossil fuel emissions as well as Houghton (2003) for land use change emissions with a total of 418 Pg C during the period 1860–1999 and, following the SRES A2 scenario, with a total of 1,770 Pg C during the twenty-first century. In the first simulation, the climate-carbon cycle feedback is taken into account, so that anthropogenic CO₂ acts on the carbon cycle and, as a greenhouse gas, on the climate. Following the usual terminology, this model run is hereafter called ‘coupled’. In the second simulation (‘uncoupled’) greenhouse warming is suppressed by fixing the CO₂ concentration in the radiation code to the pre-industrial value of 286 ppm, so that anthropogenic CO₂ affects only terrestrial photosynthesis, stomatal conductance and the ocean carbon cycle under fixed climate conditions, e.g. SST and circulation. Accordingly, the difference in surface CO₂ fluxes between both runs reflects the impact of greenhouse gas warming on the carbon cycle. Raddatz et al. (2007) proved the present carbon cycle of the coupled simulation of our study. Both simulations of this study are part of the Coupled Carbon Cycle Climate Model Intercomparison Project (C4MIP). Friedlingstein et al. (2006) examined the eleven coupled climate-carbon cycle models of this project, including the MPI-ESM on a global scale. They found that the MPI-ESM

land/ocean storage sensitivities to climate and CO₂ show only little differences from the mean and are within the standard deviations of the eleven models.

3 Methods

Besides examining the CO₂ fluxes of the coupled simulation and the differences between the coupled and uncoupled run, we present the climate change effects of those quantities, which determine the air–sea CO₂ flux. The exchange of CO₂ at the interface of the atmosphere and the ocean (F_{CO_2}) is described by:

$$F_{\text{CO}_2} = S \cdot K_w \cdot \Delta P_{\text{CO}_2} \quad (1)$$

Here, $\Delta P_{\text{CO}_2} = P_{\text{CO}_2(\text{atm})} - P_{\text{CO}_2(\text{oce})}$ denotes the difference of the CO₂ partial pressure between the atmosphere ($P_{\text{CO}_2(\text{atm})}$) and the ocean ($P_{\text{CO}_2(\text{oce})}$). According to Weiss (1970, 1974), the solubility (S) of CO₂ in ocean water is described by

$$\ln S = A_1 + A_2 \cdot (100/T) + A_3 \cdot \ln(T/100) + s \cdot [B_1 + B_2 \cdot (T/100) + B_3 \cdot (T/100)^2] \quad (2)$$

Here, T is temperature in °C and s is salinity in ‰. The A_i and B_i are from Weiss (1974). The gas transfer velocity (K_w) is:

$$K_w = (1 - F_{\text{ice}}) \frac{u^2}{(S_c/660)^{1/2}} \cdot 0.337 \quad (3)$$

Here, F_{ice} represents sea ice coverage, u wind speed and S_c the Schmidt's number. K_w is proportional to the square of the wind speed and to the fraction of the water free of sea-ice. CO₂ flux over ice is inhibited. The solubility (S) takes into account that most of the CO₂ that is taken up by the ocean is subsequently dissolved in the water accompanied by a reduction of the partial pressure of CO₂ in the water. The solubility is high/low, when temperature is low/high, i.e. cold water takes up more CO₂ than warm water.

In order to separate the effects of changing solubility, gas transfer velocity and partial pressure difference on CO₂ flux, we developed the following equation:

$$\Delta F = \Delta S \cdot \overline{K_w} \cdot \overline{\Delta P_{\text{CO}_2}} + \Delta K_w \cdot \overline{S} \cdot \overline{\Delta P_{\text{CO}_2}} + \Delta(\Delta P_{\text{CO}_2}) \cdot \overline{K_w} \cdot \overline{S} \quad (4)$$

Here, “ Δ ” denotes the difference and “ $\overline{\quad}$ ” the arithmetic mean of the coupled and the uncoupled simulation. The terms

$$\Delta F_S = \Delta S \cdot \overline{K_w} \cdot \overline{\Delta P_{\text{CO}_2}} \quad (5)$$

$$\Delta F_{K_w} = \Delta K_w \cdot \overline{S} \cdot \overline{\Delta P_{\text{CO}_2}} \quad (6)$$

$$\Delta F_{\Delta P_{\text{CO}_2}} = \Delta(\Delta P_{\text{CO}_2}) \cdot \overline{K_w} \cdot \overline{S} \quad (7)$$

describe the effects of changing solubility, gas transfer velocity and partial pressure difference, respectively on the CO₂ flux. We calculated the solubility (Eq. 2) and the terms of Eqs. 5–7 from the annual mean SST, surface salinity, gas transfer velocity and partial pressure difference.

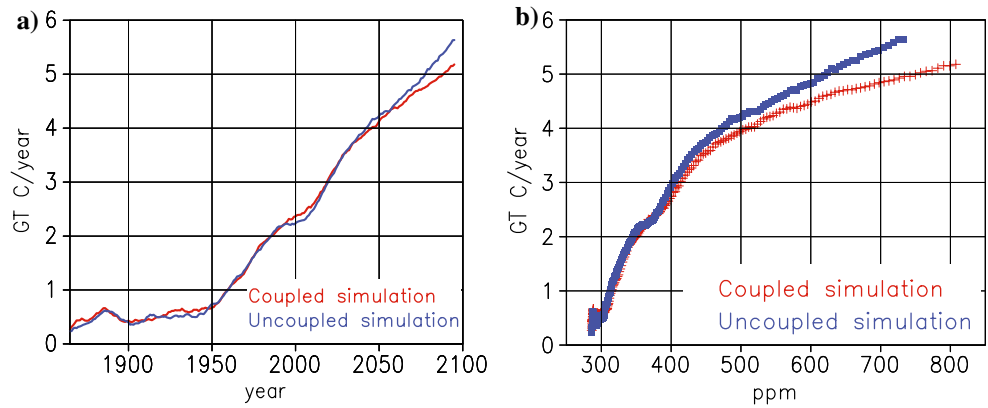
Parts of this study are based on the analysis of the differences between the coupled and the uncoupled simulation averaged for the last three simulation decades from 2070 until 2099 (hereafter the 21C decades). For all the difference maps we applied a non-parametric significance test using 30-year means. Since the pre-industrial control run consists of only 150 years, i.e. five 30-year chunks, we also utilized the first 90 years of the two transient runs. The transient simulations between 1860 and 1950 are suitable for the test, because the trend during this period is small and can be neglected. The altogether 330 simulation years were then split into 11 chunks of 30 years and differences between all chunks were calculated. The null hypothesis states that the difference between the two transient simulations is within the range of differences between randomly chosen 30-year chunks. We reject this hypothesis if the actual difference is larger than the 95% percentile of control differences. This test has been previously described and applied by Roeckner et al. (2006).

4 Results

4.1 CO₂ fluxes

In the following, we investigate the total CO₂ fluxes, comprising the natural as well as the anthropogenic fluxes. This way we account for the impact of climate change on the total fluxes. As mentioned above, a few studies concluded that the ocean's response to climate change is small compared to that of the land (e.g. Raddatz et al. 2007; Friedlingstein et al. 2006). This can be inferred from Fig. 1a, displaying the temporal evolution of the annual oceanic CO₂ uptake in the coupled and the uncoupled simulation. Not until the last decades of the simulation period notable differences between both simulations are obtained, indicating a small response of the ocean to climate change. However, in our simulations, changes of the oceanic CO₂ uptake are not only a response of the ocean to climate change but also to increased atmospheric CO₂ due to the rapid land's response to climate change (Raddatz et al. 2007; Friedlingstein et al. 2006). The terrestrial effect enhances the increase of atmospheric CO₂, forcing the ocean to an increased influx and decreased outgassing, respectively, since the air–sea CO₂ flux is proportional to ΔP_{CO_2} (Eq. 1). Thus, if the terrestrial CO₂ uptake decreases due to global warming, as in our simulation, more CO₂

Fig. 1 Annual ocean CO₂ uptake (10-year running mean), **a** against time, **b** against atmospheric CO₂ concentration (Gt C/year)



remains in the atmosphere, favoring a net CO₂ flux into the ocean. This terrestrial effect potentially partly compensates the climate change effect. In order to account for this, the oceanic CO₂ uptake is shown as a function of atmospheric CO₂ for both transient simulations. Fig. 1b reveals that for an atmospheric CO₂ concentration below 400 ppm both simulations are characterized by the same amounts of ocean CO₂ uptake and show a strong slope, indicating a strong increase of oceanic uptake with increasing atmospheric CO₂. For higher CO₂ concentrations, the curves tend to diverge with a smaller slope in the coupled than in the uncoupled simulation. This means that a given oceanic CO₂ uptake is obtained for different atmospheric CO₂ concentrations in the two simulations, which can only be attributed to climate change. For high atmospheric CO₂ levels, the same amount of CO₂ uptake is obtained for an atmospheric CO₂ concentration that is about 25% higher in the coupled than in the uncoupled simulation, reflecting the diminished ability of the ocean in the coupled simulation to take up CO₂.

4.1.1 CO₂ flux patterns

Figure 2a shows the mean annual air–sea CO₂ fluxes for the nineteenth century decades (19C, 1860–1889) of the coupled simulation. This pattern is nearly identical to that of the uncoupled simulation since climate change is negligible up to that time (not shown). The map shows the well-known CO₂ flux pattern, characterized by oceanic uptake at high northern latitudes and an out-gassing of CO₂ to the atmosphere in the Equatorial Pacific (Takahashi et al. 2002; Wetzel et al. 2005). In the course of time the ocean uptake increases. Figure 2b shows the mean CO₂ flux for the coupled simulation for the 21C decades. Over the entire oceans the CO₂ uptake is increased as a result of enhanced anthropogenic emissions, or the release of CO₂ to the atmosphere is reduced, e.g. in the Equatorial Pacific. Compared to 19C the highest flux changes occur in the Southern Ocean. The uncoupled simulation shows a similar structure (not shown). However, the difference map between both simulations for the 21C period (Fig. 3) shows

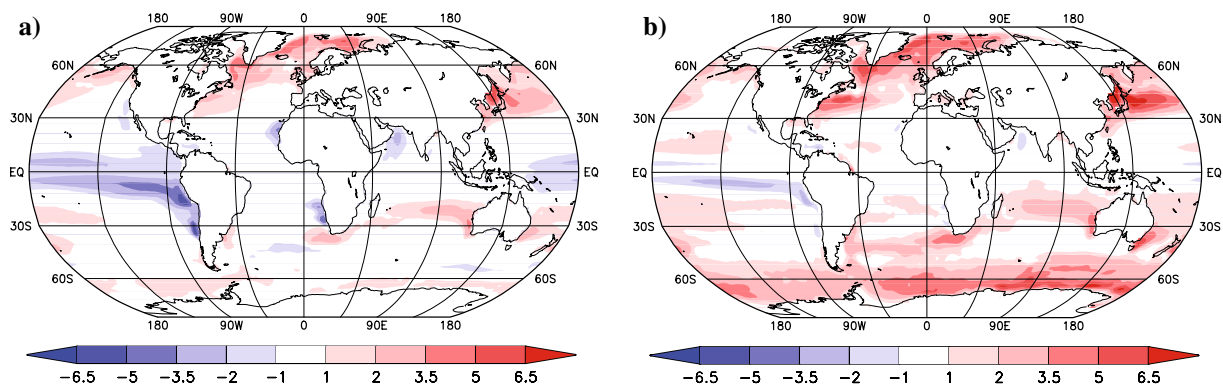


Fig. 2 Atmosphere/ocean CO₂ flux in the coupled simulation. Average period: **a** 1860–1889, **b** 2070–2099. Positive values represent ocean uptake (mol m⁻² year⁻¹)

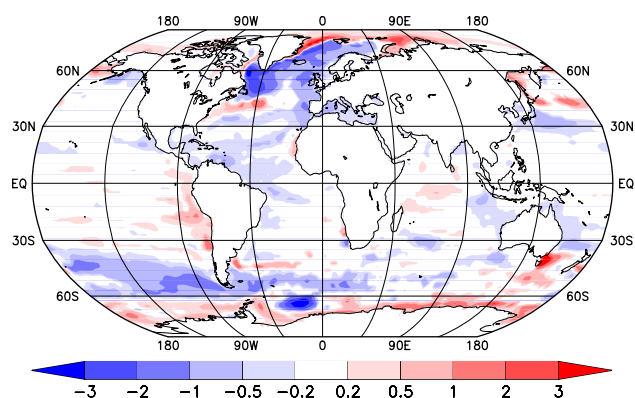


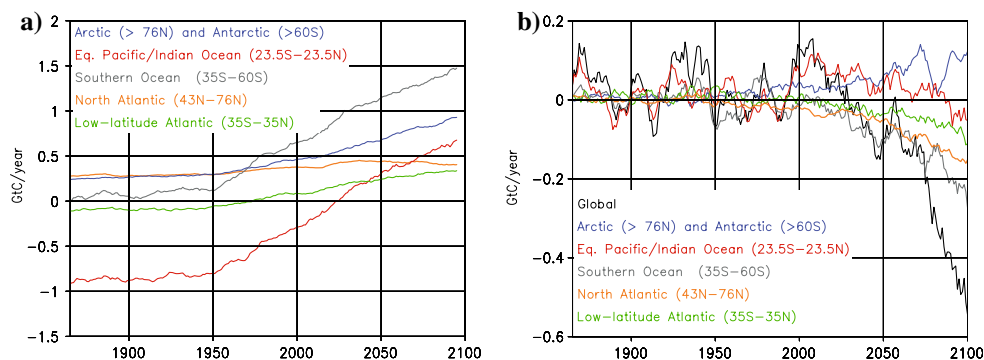
Fig. 3 Atmosphere/ocean CO₂ flux: Difference between the coupled and the uncoupled simulation. Average period: 2070–2099. Negative values (blue) represent less oceanic uptake in the coupled simulation. Only significant values at the 95% level are shown (mol m⁻² year⁻¹)

a pronounced pattern: Positive values appear in the Southern Ocean south of 60°S, in the North Pacific, south of Australia and especially in the Greenland and Barents Sea, whereas climate change leads to reduced ocean CO₂ uptake especially in the North Atlantic, in the Southern Ocean (35°S–60°S) and in the Weddell Sea. At low latitudes statistically significant reductions are simulated mainly in the Atlantic Ocean (only values significant at the 95% confidence level are shown).

4.1.2 Regional CO₂ fluxes in the coupled simulation

In the following, we investigate in detail the fluxes for those areas with significant large-scale changes in CO₂ flux: the North Atlantic (43°N–76°N) (hereafter NA), the low-latitude Atlantic (35°S–35°N) (hereafter LLA), the Equatorial Pacific and Indian Ocean (23.5°S–23.5°N) (hereafter EQPI), the Southern Ocean (35°S–60°S) (hereafter SO) and the Arctic (>76°N) and Southern Ocean around Antarctica (>60°S) (hereafter AAO). Figure 4a shows the annual mean spatially integrated CO₂ fluxes for

Fig. 4 Spatially integrated annual atmospheric/ocean CO₂ uptake (10-year running mean) (positive values indicate oceanic CO₂ uptake), **a** Coupled simulation, **b** Coupled minus uncoupled simulation (Gt C year⁻¹)



the above-mentioned areas in the coupled simulation. At the end of the twenty-first century, the area with the highest uptake is the SO. Whereas the fluxes are small in the nineteenth century, an uptake of about 1.5 Gt C/year is simulated at the end of the twenty-first century. The second area that strongly contributes to the global increase in oceanic CO₂ uptake of about 5 Gt C/year in 2100 (cf. Fig. 1a) is the EQPI. Here, the out-gassing of about 0.8 Gt C/year before 1950 is steadily reduced in the following decades resulting in a net uptake from around 2025 onward. At the end of the twenty-first century, the uptake is about 0.7 Gt C/year. Thus, the total contribution from the EQPI region to the global CO₂ flux change is about 1.5 Gt C/year. The AAO and the LLA regions also contribute to the increase in oceanic CO₂ uptake. AAO increases the uptake from 0.25 Gt C/year in 1860 to 0.9 Gt C/year in 2100, the LLA from small negative values in 1860 (–0.1 Gt C/year) to 0.3 Gt C/year in 2100. In the NA the CO₂ uptake only increases from 0.25 to 0.4 Gt C/year (cf. Fig. 2).

The residuum of the fluxes, i.e. the difference between the global fluxes and the total sum of the regional fluxes discussed above, only shows a small increase in CO₂ uptake and is not further discussed here.

4.1.3 Impact of climate change on global and regional CO₂ fluxes

The globally integrated difference between the coupled and the uncoupled simulation (Fig. 4b) is characterized by a nearly unchanged behavior until the beginning of the twenty-first century and a sharp decrease in the last simulation decades. This leads to an additional heightening of atmospheric CO₂, thus representing a positive feedback between oceanic CO₂ uptake and atmospheric CO₂ concentrations. The decrease of ocean CO₂ uptake is more than 0.5 Gt C/year until 2100 in the coupled simulation compared to the uncoupled simulation. This is about 10% of the total uptake in the coupled simulation (cf. Fig. 1a). The SO

region, representing 20% of the global ocean area, accounts for 0.25 Gt C/year difference in CO₂ fluxes, which is half of the global difference between both simulations in 2100. Remarkably, the NA region contributes a significant proportion to the difference between the coupled and the uncoupled simulation (0.16 Gt C/year), although the absolute increase obtained for both simulations is relatively small (Fig. 4a). In fact, about one third of the global difference between both simulations is due to changes in the NA, representing only 5% of the ocean's surface. A negligible net response to climate change is found in the EQPI region. Here, the decrease of the CO₂ uptake in the uncoupled run during the last simulation decades is within the variability of the first decades. This could be also expected from Fig. 3, which only shows little statistically significant CO₂ flux differences in the Equatorial Pacific and Indian Ocean. In contrast, in the AAO a negative feedback mechanism between atmospheric CO₂ concentration and CO₂ flux is evident: At the end of the twenty-first century an additional CO₂ uptake is simulated in the polar areas that makes up about 20% of the global CO₂ flux decrease, thus partly masking it (Note that this integrated value also includes the Weddell Sea, where decreased ocean uptake is found. Thus, the masking effect would be even higher if we had removed the Weddell Sea from the analysis).

4.2 CO₂ flux determining properties

The various temporal changes, amounts and directions of CO₂ flux changes indicate that there are different feedback mechanisms between atmospheric CO₂, climate and oceanic CO₂ uptake acting in different areas. In the following, the changes of quantities affecting CO₂ fluxes according to Eqs. 4–7 will be exploited. Namely, we examine the differences between the coupled and the uncoupled simulation averaged from 2070 until 2099.

4.2.1 Solubility

According to Eqs. 1 and 2, solubility is one parameter that determines the atmosphere/ocean CO₂ flux in dependence mainly on SST and secondary on salinity. The dissolution of CO₂ in the ocean implies that the atmosphere only ‘sees’ a small fraction, namely the gaseous CO₂ of the total carbon in the surface layer. Thus, the CO₂ partial pressure difference between ocean and atmosphere is maintained. Subsequent vertical transport of the carbon-enriched water removes carbon from the surface layers. Figure 5 reveals that climate change leads to a decrease of solubility, predominantly north of 40°N and, to a smaller extent, south of

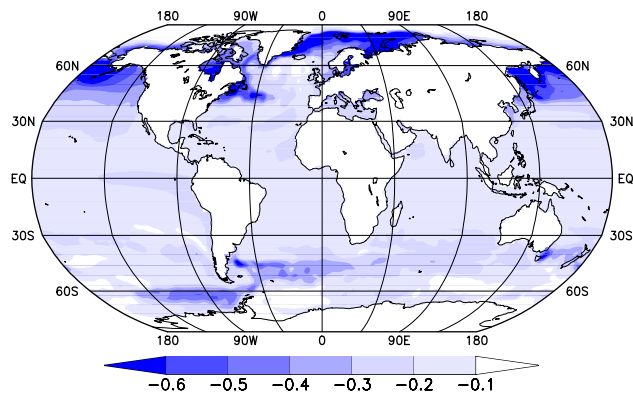


Fig. 5 Solubility: coupled minus uncoupled simulation. Average period: 2070–2099. Only significant values at the 95% level are shown (10^{-2} moles kg^{-1} atm^{-1})

40°S. These solubility reductions are mainly caused by the SST rise (Fig. 6). Globally, the annual mean SST increases by about 2.2 K in the coupled simulation compared with the uncoupled simulation. However, the pattern of SST increase is inhomogeneous and reflects partly ocean dynamics: In areas with vertical mixing and convection, like the Southern Ocean and the North Atlantic, the SST increase is generally smaller or even negligible. In the North Atlantic, the pattern also mirrors the slowdown of the North Atlantic meridional overturning circulation (MOC) (cf. Fig. 15 and Sect. 4.3.2). Maximum SST increases of 5 K are found in the North and the Northwest Pacific, the Greenland and the Barents Sea. Here, also the main decreases of solubility are obtained. SST considerably increases also in the Equatorial oceans, which do not lead to remarkable changes of solubility. The reason for that is that a given SST increase leads to a smaller solubility decrease on high temperature than on low temperature levels (Eq. 2; Weiss 1974). In contrast to the Equatorial Oceans, a moderate warming of the cold Southern Ocean (south of 30°S) leads partly to a clearly reduced solubility.

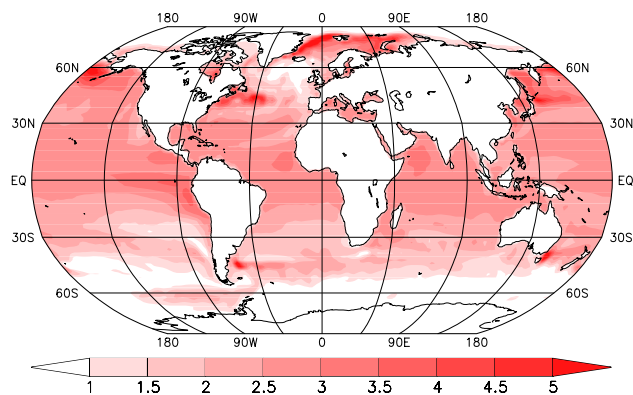


Fig. 6 Same as Fig. 5: for SST (°C)

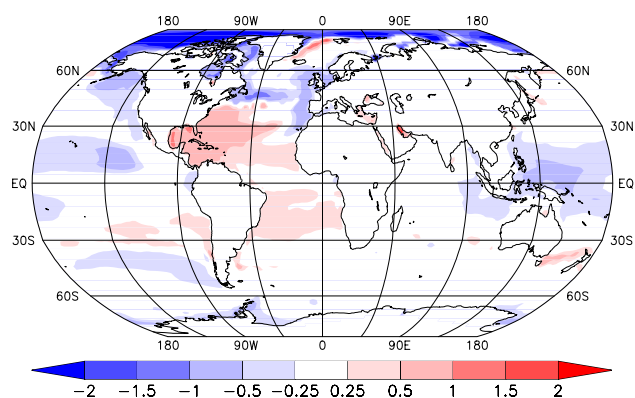


Fig. 7 Same as Fig. 5: for salinity (‰)

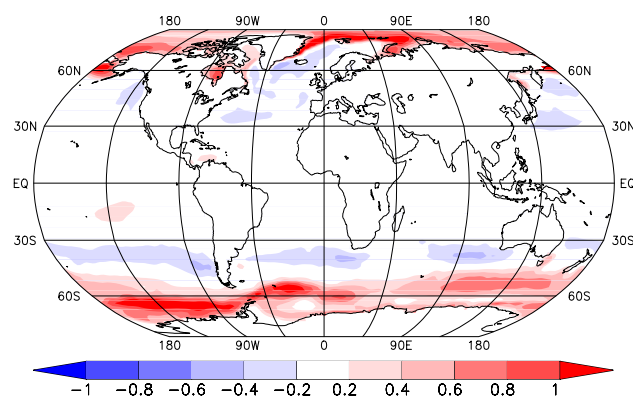


Fig. 8 Same as Fig. 5: for CO₂ gas transfer velocity (K_w) (10^{-9} mol m^{-2} s^{-1} ppm^{-1})

Compared with SST, salinity is of secondary importance for solubility. An increase of salinity leads to a decrease of solubility and vice versa. Changes of salinity mainly reflect precipitation and evaporation changes as well as sea ice melting. The latter is suggested to lead to strongly decreased salinities in the Arctic (Figs. 7, 9). Another dominant feature of salinity is its increase in the north-western Subtropical Atlantic, while in the western Equatorial Pacific area salinity shows lower values in the coupled simulation than the uncoupled simulation. The increase in the low-latitude Atlantic tends to reduce solubility, while the salinity decrease in the east Equatorial Pacific slightly counteracts the temperature effect (Fig. 6).

4.2.2 Gas transfer velocity

The gas transfer velocity K_w , shown in Fig. 8, also determines the CO₂ flux. Significant increases of K_w are only found in the higher latitudes, especially in the Arctic Ocean and the Southern Ocean. According to Eq. 3 K_w variability is a result of changing sea ice cover and wind stress (Figs. 9, 10). Melting of ice is predominantly simulated in the Arctic, where sea ice in late summer disappears at the end of the twenty-first century (not shown). In the Southern Ocean, sea ice is found to decrease especially around the Antarctic Peninsula and the Ross Sea. In the northern hemisphere, the annual mean sea ice cover diminishes in the coupled simulation compared to the uncoupled simulation by 45%. In the southern hemisphere, the annual mean sea ice cover is reduced by 36%. Consequently, the period, when atmosphere/ocean CO₂ flux is possible, increases and so does the gas transfer velocity.

Wind stress changes are part of the climate change especially in the southern hemisphere, where an enhancement of the wind speed and a shift of the storm tracks and

the accompanying wind fields to the south are simulated (Fig. 10). This has previously been found for example by Bengtsson et al. (2006) and Kushner et al. (2001). Yin (2005) also investigated the poleward shift of the surface zonal wind stress of an ensemble of twenty-first century climate simulations. For ECHAM5/MPI-OM he found that the latitude of the present day maximum of zonal wind stress fits well with that of the ensemble mean in the Southern Ocean. Only a slight overestimation of the difference of zonal wind stress between 2081–2100 and 1981–2000 is obtained for ECHAM5/MPI-OM compared with the ensemble mean. This indicates that the MPI-ESM reasonably accounts for wind stress changes in the Southern Ocean, which are supposed to enhance CO₂ flux into the ocean (Russell et al. 2006). In the coupled simulation, changes of the wind fields lead to reduced wind stress around 40°S and increased wind stress between 50°S and 60°S, with a maximum around 100°E. The shift and enhancement in the coupled simulation compared with the uncoupled simulation is further demonstrated in Fig. 11. While the wind stress in the uncoupled simulation is around 0.195 Nm^{-2} , it increases in the coupled simulation to almost 0.22 Nm^{-2} in the last three decades of the twenty-first century. Besides this change of the amount, the latitude of maximum wind stress is shifted southward from 49.5° to almost 51°S. Due to these wind stress changes decreasing K_w appear around 40°S, while between around 50° and 60°S a large area with increased CO₂ gas transfer velocities emerges. Farther to the south (>60°S) the retreat of sea ice dominates the K_w changes. Wind stress changes in the northern hemisphere are not as evident. Here, the gas transfer velocity for CO₂ is mainly affected by sea ice cover reductions. On the whole, the CO₂ gas transfer velocity increases and thus favors an enhancement of CO₂ uptake provided that solubility and partial pressure difference remain constant (see Sect. 4.2.4).

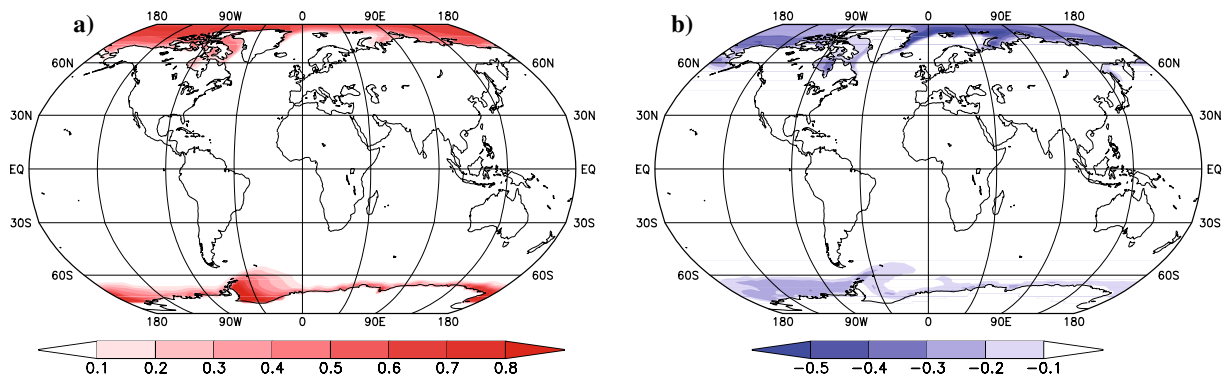


Fig. 9 Sea ice cover fraction. Average period: 2070–2099. **a** Coupled simulation, **b** coupled minus uncoupled simulation

4.2.3 Partial pressure difference

The partial pressure difference (ΔP_{CO_2}) influences not only the amount, but determines exclusively the direction of the CO₂ flux between the atmosphere and the ocean. When the partial pressure difference in the ocean is higher than that of the atmosphere, the ocean releases CO₂ to the atmosphere and vice versa. Since the atmospheric CO₂ concentration is globally almost homogenous, the spatial pattern of the partial pressure difference between the ocean and the atmosphere is predominantly determined by the oceanic partial pressure. On the whole, ΔP_{CO_2} shows a reduction in the coupled run compared with the uncoupled simulation, thus leading to a net reduction of oceanic CO₂ uptake (Fig. 12). The strongest decreases are found in the Arctic Sea, the North Atlantic and in parts of the Southern Ocean, especially in the Weddell Sea, whereas smaller reductions are mainly simulated in the South Pacific and in the low-latitude Atlantic. Some smaller areas with increased ΔP_{CO_2} are found in the upwelling zone west of the South American coast and south of Australia.

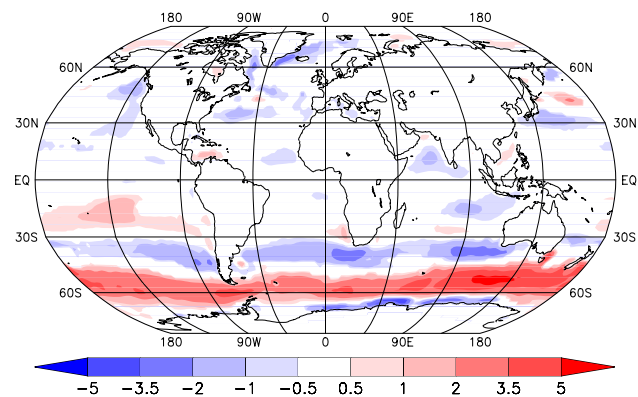


Fig. 10 Same as Fig. 5: for wind stress (10^{-5} Pa/1025)

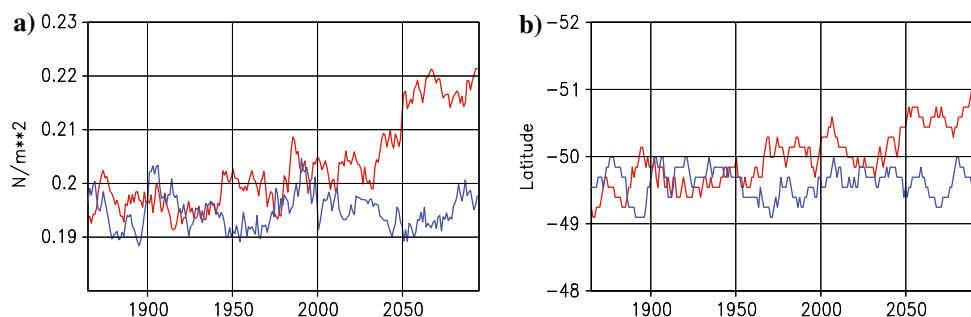
4.2.4 Global budgets

In order to quantify the global effects of the three parameters S , K_w and ΔP_{CO_2} on the climate-induced CO₂ uptake change, we calculated the temporal evolution of the terms ΔF_S , ΔF_{k_w} and $\Delta F_{\Delta P_{\text{CO}_2}}$ according to Eqs. 4–7. Figure 13 also shows the sum of the three terms, overall reflecting the features shown in Fig. 4b. Small deviations occur, since we neglect non-linearity (Eq. 4) and utilized annual mean values for the estimations shown in Fig. 13, whereas the fluxes shown in Fig. 4b are summarized for each time step. Figure 13 reveals that the climate change effect on the partial pressure difference ΔP_{CO_2} dominates the effects on solubility and gas transfer velocity. The ΔP_{CO_2} effect leads to a reduced net oceanic CO₂ uptake in the coupled compared with the uncoupled simulation of approximately 1 Gt C/year. The solubility effect also leads to a reduction of CO₂ uptake of the ocean, but it makes up only about 25% of the ΔP_{CO_2} effect (≈ 0.25 Gt C/year). The gas transfer velocity counteracts the other two terms by a positive proportion of CO₂ uptake of about 0.7 Gt C/year. Notwithstanding the contrasting effect of gas transfer velocity increase due to wind stress enhancement and sea ice melting, which lead to a substantial net oceanic CO₂ uptake, the net coupled effect on CO₂ uptake as a consequence of global warming is dominated by partial pressure difference and a secondary by solubility contributions.

4.3 CO₂ transport out of the surface layer

The strong effect of ΔP_{CO_2} changes on the reduction of CO₂ uptake induced by climate change needs further examination, whether dynamic ocean processes or biologic production account for the decrease of ΔP_{CO_2} . Therefore, we examine the maximum mixed layer depth (MLD), some main oceanic circulation features and export.

Fig. 11 **a** Maximum zonal averaged wind stress in the Southern Hemisphere; **b** latitude of maximum zonal averaged wind stress; (10-year running mean). Red coupled simulation; blue: uncoupled simulation



4.3.1 MLD

The MLD is a measure for the vertical stratification, but can also be used as an indicator for the degree of vertical mixing. Stratification is affected by density changes of the water column, induced by salinity and temperature changes. A decrease in density due to SST rise and a freshening of surface waters tend to strengthen the ocean stratification, thus leading to reduced vertical transports, e.g. up- and downward transport of CO₂ and upward transport of nutrients. In addition, wind fields may also influence the vertical mixing and convective sinking and hence MLD. Therefore, SST, salinity as well as wind field changes do not only affect the solubility and gas transfer velocity, respectively, but additionally influence the stratification of the water column, thus driving the main features of the ocean dynamics (Wunsch 2002; Stouffer et al. 2006). The MLD is a diagnostic property of the model, here defined as the depth where the density change from the ocean surface exceeds 0.125 kg/m³. The maximum MLD in the coupled simulation and the differences between the coupled and the uncoupled simulation in the 21C decades are shown in Fig. 14. The maximum MLD is shallower in the coupled than in the uncoupled simulation, which is in line with most other OAGCM simulations under global warming (e.g. Sarmiento et al. 2004; Manabe 1998). The strongest decline of maximum MLD is simulated in those areas

where the maximum MLD is deep, like the Southern Ocean and the North Atlantic. In the low latitudes, the maximum MLD is generally shallower, thus changes of the MLD are also smaller. Here, mainly the Pacific shows a significant decline of the maximum MLD. A comparison of Figs. 3 and 14b reveals that partly a strong CO₂ uptake decrease and a decline of maximum MLD coincide, especially in the North Atlantic and the Southern Ocean.

4.3.2 Meridional overturning circulation (MOC) and Antarctic circumpolar current (ACC)

The strong changes of the maximum MLD in the Southern Ocean and the North Atlantic, which coincides with the areas with the strongest CO₂ flux changes due to climate change, hints at changes of the ocean circulation as a driving factor for CO₂ flux changes due to climate change. Therefore, we briefly examine here the main dynamic features in the North Atlantic and the Southern Ocean, i.e. the North Atlantic MOC and the ACC. Figure 15a shows the difference of the North Atlantic Overturning between the coupled and the uncoupled simulation averaged from 2070 to 2099. The maximum appears at a depth of around 1,500 m between 35° and 40°N. The temporal evolution of the maximum MOC at 35°N of both simulations is shown in Fig. 15b. In the uncoupled simulation the mean value is about 21 Sv, slightly higher than the value of 18 ± 4 Sv reported in Macdonald (1998) for the present climate. Under climate change conditions, we expect a weakening of the North Atlantic MOC, as shown in former studies (e.g. Stouffer et al. 2006). Actually, after around 2000, the MOC reduces in the coupled simulation, reaching around 15 Sv at the end of the twenty-first century. The export from the Atlantic across 30°S into the Southern Ocean in the uncoupled simulation and in the first decades of the coupled simulation is about 17.5 Sv (Fig. 16). At the end of the twenty-first century, this transport reduces to around 15 Sv in the climate change simulation. Hence there is not only a weaker circulation in the North Atlantic, but also the Atlantic transport in the Southern Ocean is reduced, indicating a weakening of the Atlantic contribution to the

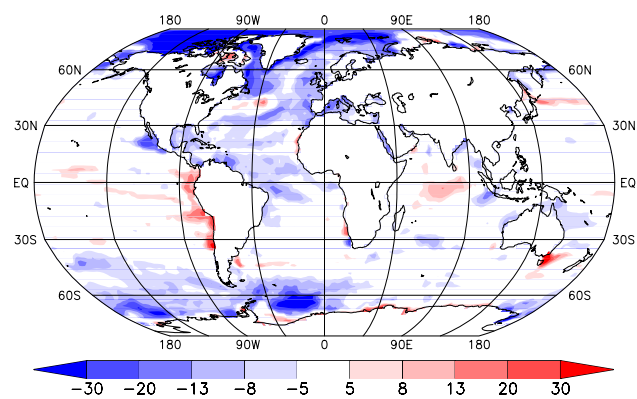


Fig. 12 Same as Fig. 5: for ΔP_{CO_2} (ppm)

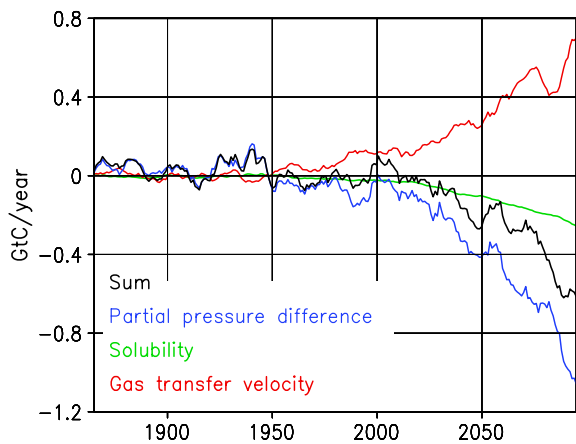


Fig. 13 Global budgets of ΔF_s (green), ΔF_{kw} (red), $\Delta F_{\Delta PCO_2}$ (blue) and sum of all three terms (black); see also Eqs. 5, 6, 7 (Gt C year⁻¹); (10-year running mean)

ocean circulation in the southern hemisphere. In the Southern Ocean the ACC is the dominant feature, clockwise circulating around Antarctica. A measure of the ACC is the mass flux through Drake Passage. We calculated the mass flux from the barotropic streamfunction (Fig. 17). In the uncoupled simulation the mean flux is 169 Sv, which is about 20% higher than observational estimates, but hardly higher taking into account the error of average transport of 15–27 Sv (Cunningham et al. 2003). Under climate change, no remarkable changes of the ACC are evident compared with the uncoupled simulation. In both simulations the variability is high, not allowing an assessment of the high values in the last decades of the twenty-first century in the coupled simulation. Thus, clearer signals, whether the coupled simulation also leads to an increase of the ACC, which has been reported by e.g. Fyfe and Saenko (2005) and Russell et al. (2006) in the twenty-second and the twenty-third century are likely to be found in longer simulations only.

4.3.3 Export

In addition to the vertical transports of CO₂ (solubility pump), the biological pump—expressed as export—removes carbon out of the euphotic zone (upper 80–100 m) into the deeper layers and reduces ($P_{CO_2(occ)}$). This finally leads to a vertical gradient of dissolved inorganic carbon (DIC) with low values in the surface layers and high values in deep layers (Sarmiento 1992). Globally integrated, the export is reduced in the coupled simulation by 8% compared to the uncoupled run in the 21C. Similar changes are found for photosynthesis (−8%), phytoplankton (−7%) and zooplankton (−8%). Figure 18 shows the export for the 21C decades. The maps for the absolute as well as for the difference values show the highest amounts in the low latitudes, i.e. mainly in those areas, where no strong CO₂ flux changes occur (Fig. 3). Only in the Atlantic between 30°S and 30°N the export change is in line with the CO₂ flux changes. In the Pacific and Indian Ocean reduced export is found, but no significant CO₂ flux changes (Fig. 4). The reduced export in these areas is coincident with reduced supply of the nutrients phosphate and nitrate (not shown). A reduction of export due to climate change is expected, since the reduced vertical mixing leads to less transport of nutrients to the upper layers. This obviously happens in the Equatorial Pacific, where reduced nutrients as well as reduced maximum MLD are simulated (Fig. 14). However, this explanation cannot account for the reduced export in the low-latitude Atlantic, which is accompanied by reduced nutrients, but not by significant MLD changes. Around 50°S, between 0° and 180° E we find a band with small export reductions, which are not related to reduced nutrients. We assume that the reason for that is the decreased light supply due to increased cloud cover, which is accompanied by the poleward shift and intensification of the wind stress belt (Fig. 10) under climate change conditions. Slightly increased export is found especially in the

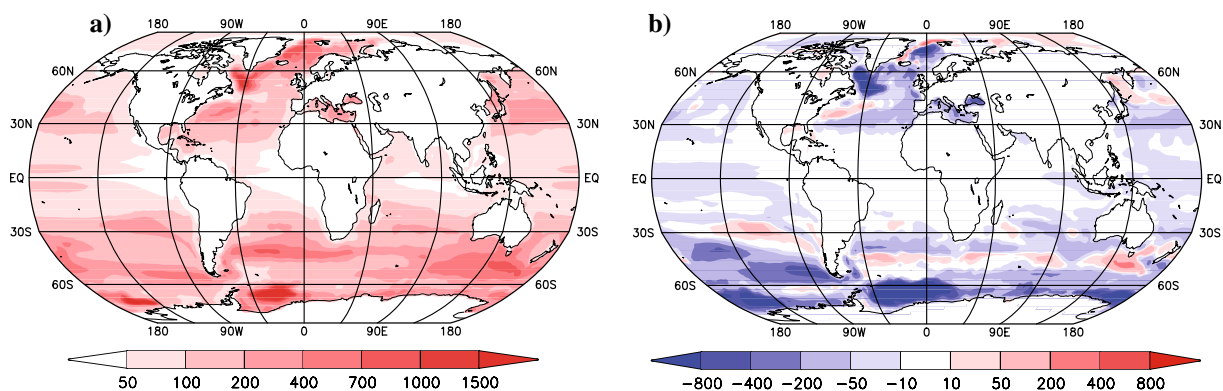
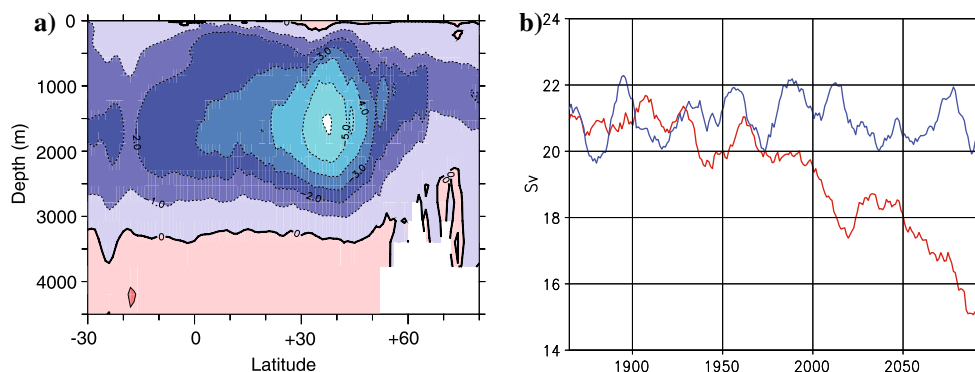


Fig. 14 Maximum mixed layer depth. Average period from 2070 to 2099. **a** Coupled simulation, **b** coupled minus uncoupled simulation (m)

Fig. 15 a Atlantic meridional overturning streamfunction; coupled minus uncoupled simulation; average period from 2070 to 2099 (Contour interval is 1 Sv), **b** strength of annual mean Atlantic meridional overturning streamfunction at 35°N (red coupled, blue uncoupled simulation, (10-year running mean))



Arctic. This coincides with the retreat of sea ice in the coupled simulation. Since the model inhibits light penetration below sea ice, melting increases the solar radiation in the upper water layer, thus enhancing primary production. However, since there is anyway only limited light supply in these high latitudes, biological production and export in the polar areas are also limited.

5 Discussion

We evaluate the response of the ocean within the feedback system of CO₂ emissions, atmospheric CO₂ concentrations, climate change and CO₂ uptake of the terrestrial biosphere and the ocean. As in previous studies, there is a positive feedback between the ocean and atmospheric CO₂ concentrations: global warming induced by an increase of atmospheric CO₂ leads to a reduction of oceanic CO₂ uptake, thus further increasing the atmospheric CO₂ concentration. The response of the ocean is evident not until the last decades of the twenty-first century, the end of our simulation. At the end of the twenty-first century, the global ocean CO₂ uptake in the coupled simulation has decreased by around 10% compared with the uncoupled

simulation. This includes the response of the ocean to increased atmospheric CO₂ concentrations due to the faster and stronger response of the land biosphere (more than 80% of the total response) to global warming.

The CO₂ uptake of the ocean, its response to global warming and the underlying processes found in our simulations are different in the different parts of the world ocean. Globally averaged, the main net decrease is provided by the partial pressure difference between atmosphere and ocean. This contribution even exceeds the total of the ocean's response to climate change. Solubility also contribute to a decrease of CO₂ flux into the ocean, its proportion is however only about 25% of the partial pressure difference proportion. These two effects are to a large degree offset by gas transfer velocity effects, resulting from changes of the wind stress fields in the Southern Ocean and from sea ice melting in the Arctic and Antarctic Ocean. These global results are also mirrored by the maps for solubility, gas transfer velocity and partial pressure difference changes (Figs. 5, 8, 12). Over large areas, the ΔP_{CO_2} differences between both simulations reflect the CO₂ flux differences in the 21C period (Figs. 3, 12). Significant deviations between Figs. 3 and 12 are obtained in the Arctic and around Antarctica, where CO₂ flux changes

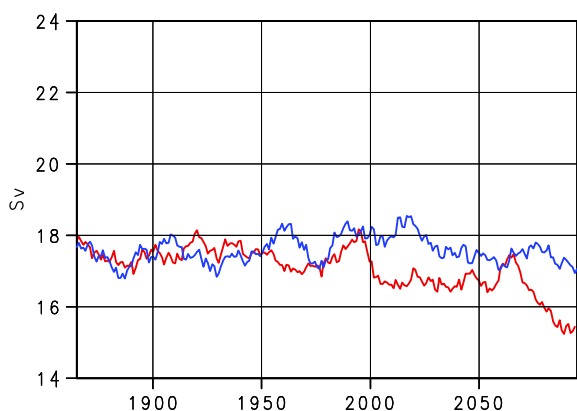


Fig. 16 Transport volume from the Atlantic across 30°S (red coupled, blue uncoupled simulation), (10-year running mean)

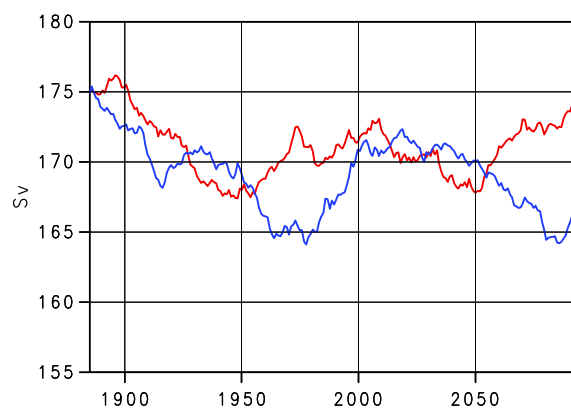


Fig. 17 Strength of Antarctic Circumpolar Current at the Drake Passage; red coupled, blue uncoupled simulation (Sv); (10-year running mean)

are in line with increases of the gas transfer velocity K_w . In these areas, K_w changes are owing to the retreat of sea ice (Figs. 8, 9), whereas between 30° and 60°S K_w mirrors the changes of the wind fields (Figs. 8, 10). South of around 50°S, both effects lead to large areas with increased CO₂ gas transfer velocities, favoring an enhancement of CO₂ uptake and thus competing with the effects from reduced ΔP_{CO_2} and solubility. Wind stress changes in the northern hemisphere are not so strong, thus do not strongly affect the gas transfer velocity for CO₂.

The Southern Ocean between 35° and 60°S (SO) accounts for half of the total global CO₂ flux difference between both simulations. Especially in the Pacific area of the SO the CO₂ flux pattern is in good agreement with that of ΔP_{CO_2} (Figs. 3, 12) and the maximum MLD (Fig. 14b), highlighting the dominant role of ΔP_{CO_2} reductions in determining the CO₂ fluxes, which in turn results from a reduction of the maximum MLD. CO₂ gas transfer velocity changes, which are mainly related to wind stress changes in the SO (30°–60°S), only partly reflect the changing CO₂ fluxes, e.g. south of Australia. This indicates that the effect of the wind stress does not dominate the changes in CO₂ uptake even in the SO, although in this area pronounced wind stress increases occur (Figs. 3, 10). The second largest response to climate change is provided by the North Atlantic. Here, areas with reduced CO₂ fluxes correspond with those where the maximum MLD is reduced, especially in the Labrador Sea and the Greenland/Norwegian Sea, suggesting a decrease of CO₂ transports into deeper layers (Figs. 3, 14b). The reduced maximum MLD in the North Atlantic is associated with a reduction of the MOC from 21 Sv to around 15 Sv, leading to a decrease of North Atlantic Deep Water formation and of the export volume from the Atlantic into the Southern Ocean from 17.5 to 15 Sv (Figs. 15, 16). Thus, we expect a reduction of carbon transport in the layers between 2,000 and 3,000 m along the southward pathway of these water masses. Actually, the DIC concentration between 2,000 and 3,000 m shows reductions

mostly pronounced in the North Atlantic and furthermore along the East American coast across 30°S (Fig. 19a).

The strong response of CO₂ flux to climate change in the North-Atlantic is remarkable, especially under consideration of its small response to the increase of atmospheric CO₂ compared with other areas, e.g. the Southern or Equatorial Oceans. We suggest that the weak response of the North Atlantic to rising atmospheric CO₂ content is due to a limited capability of the North Atlantic to take up CO₂ under stable circulation conditions. Under fixed climate conditions, solubility and gas transfer velocity remain nearly constant. Therefore, in order to provide a small CO₂ flux into the ocean, changes of ΔP_{CO_2} remain small; hence the oceanic partial pressure difference almost similarly rises as the atmospheric partial pressure does. This implies that the transport of CO₂ into deep layers does not considerable increase. Since in the North Atlantic the amount of detritus export is small, we assume that the CO₂ flux is driven and directly related to the North Atlantic MOC. In the coupled simulation the MOC is reduced by about 30% compared with the uncoupled simulation, which is the similar proportion of CO₂ flux decrease into the ocean (Figs. 4a, b, 15b). Summarized, in the North Atlantic the CO₂ uptake hardly increases as long as the MOC is stable, even if atmospheric CO₂ concentration is high. A reduced MOC, however, subsequently leads to a reduced CO₂ flux into the ocean.

In the Arctic and Southern Ocean (south of 60°S) (AAO), enhanced oceanic CO₂ uptake is simulated, especially pronounced in the Greenland and the Kara Sea, where a strong temperature increase leads to a drastic reduction of sea ice, less inhibiting CO₂ fluxes and thus increasing gas transfer velocity (Figs. 3, 6, 9). Additionally, sea ice melting leads to increased insolation of the water, favoring an increase of detritus export (Fig. 18b). Thus, in these areas, contributions from a higher CO₂ gas transfer velocity, export and mixing (Greenland and Kara Sea) accumulate and over compensate solubility effects.

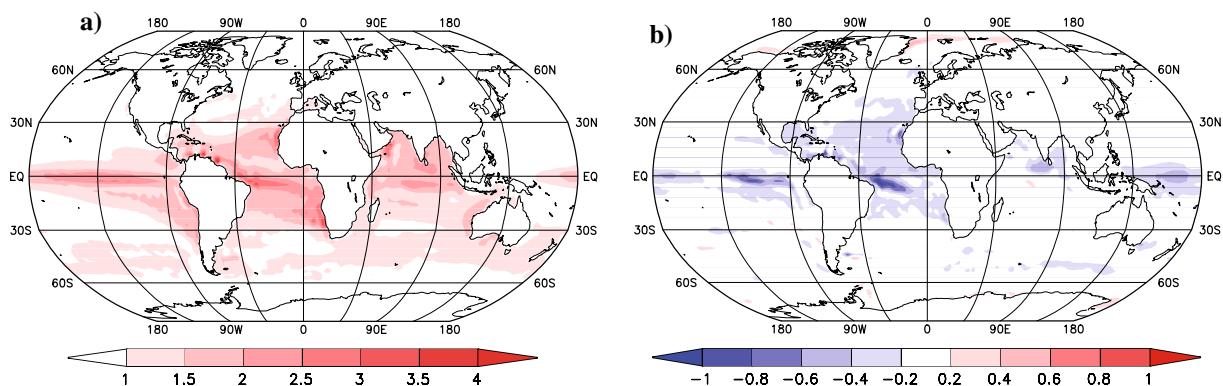


Fig. 18 Export of detritus; average period from 2070 to 2099. **a** Coupled simulation, **b** coupled minus uncoupled simulation ($\text{mol m}^{-2} \text{year}^{-1}$)

Compared with the low-latitude oceans, biological production remains small in the AAO because of the insufficient light supply. In our model this leads inevitably to decreasing photosynthesis in these high latitudes, since our model does not account for any light acclimation. Also in the Weddell Sea, a strong decrease of CO₂ uptake is simulated in the coupled run. This area is characterized by a large MLD in the coupled as well the uncoupled simulation, associated with strong deep convection and the formation of Antarctic bottom water. Deep convection acts as an effective pump removing CO₂ from the surface and transporting it into deep layers. Thus, the strong reduction of the maximum MLD in the coupled simulation compared with the uncoupled simulation (Fig. 14) indicates a slow-down of deep convection and consequently reduction of vertical CO₂ transport into deep layers. This is confirmed by the concentration of DIC in deep layers. Between 4,000 and 5,700 m, representing the depth of the Antarctic Bottom Water, the difference of DIC between both simulations reveals the highest reductions in the Weddell Sea, where a maximum of MLD decrease appears (Figs. 14, 19b).

In the equatorial oceans, the CO₂ fluxes strongly increase in both simulations (Fig. 4a). Their differences and hence the climate change effect are small and statistically significant only in the low-latitude Atlantic (LLA) and south of Indonesia with a smaller CO₂ flux and near the west coast of South America with a higher CO₂ flux in the coupled simulation than in the uncoupled simulation (Figs. 3, 4b). Reduced export is obtained in the LLA, which is in line with reduced nutrient supply in this area. We suggest that the reduced CO₂ fluxes in the LLA result from accumulated effects of reduced solubility and biological production (Figs. 5, 18b). Another remarkable feature of the LLA is the increase of salinity, opposing and probably partly offsetting the stratification effect of increasing temperature and leading at most to insignificant maximum MLD changes (Figs. 6, 7, 14b). However, this

temporally stable MLD can therefore not account for the reduced nutrient supply. Thus, we cannot fully explain the processes in the LLA. In the Equatorial Pacific and Indian Ocean (EQPI) (except the upwelling zone near the west coast of South America), no statistically significant CO₂ flux changes are found despite the export shows partly significant decreases, especially near the Equator. We assume that, owing to the strongly increased SST in the coupled simulation, the upwelling of CO₂-rich water from deep layers is weakened, compensating for the reduced CO₂ fluxes due to the biological pump in the EQPI (Figs. 3, 6, 18b).

The strongest response of biology to climate change is confined to the equatorial oceans, thus in areas, where the CO₂ flux response to climate change is small. Thus, we conclude that in our simulations, the response of biology to climate change is of secondary order. However, in our simulations biological production is iron-limited, which leads to a limited export, as long as iron concentration is low. This is predominantly the case in the Southern Ocean, where the supply with dust is small. Dust predominantly originates in the Sahara and thus mainly provides the Atlantic Ocean with iron.

The response of the oceanic CO₂ uptake to climate change has been exploited in other studies, which on the whole show that the ocean takes up less CO₂ under global warming compared to a fixed climate simulation. Ocean-atmosphere general circulation models, coupled to land and oceanic carbon models generally show less ocean CO₂ uptake than those models, which are not coupled with a terrestrial carbon cycle module (Cox et al. 2000; Dufresne et al. 2002; Friedlingstein et al. 2006). The reason for that is that the increased atmospheric CO₂ concentration leads to a rapidly decreased land uptake, which in turn further increases the atmospheric CO₂ content. This effect compensates the oceanic response to climate change, which is also the case in our coupled simulation. The area with the

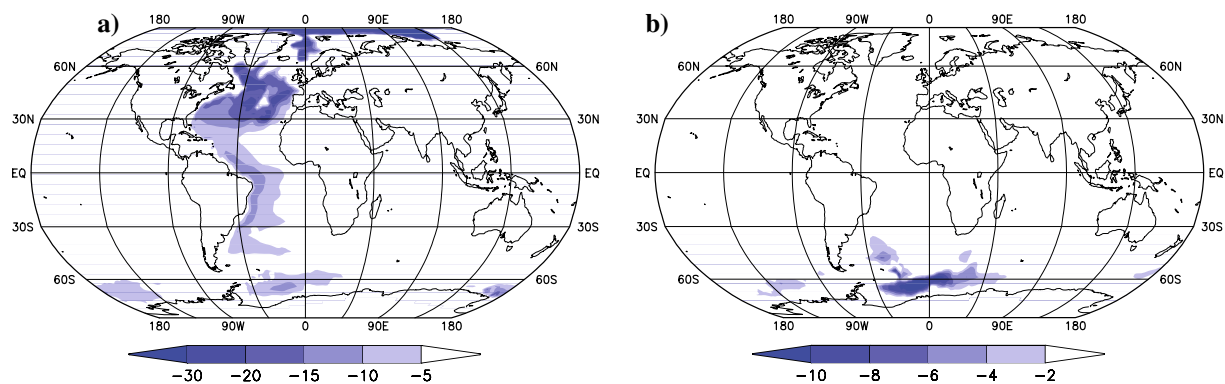


Fig. 19 Total dissolved inorganic carbon (DIC); coupled minus uncoupled simulation; average period: 2070–2099. Depth: **a** 2,000–3,000 m, **b** 4,000–5,700 m (mol m^{-2})

strongest response to climate change in our simulations is the Southern Ocean. Except for the area around the coast of Antarctica we find a decrease of CO₂ uptake south of 35°S, which mainly mirrors the shallower mixed layer. This is in line with Sarmiento et al. (1998), who examined simulations with a coupled atmosphere–ocean model until 2065. They found that climate change leads to surface freshening and enhanced stratification in the Southern Ocean, which subsequently lead to decreased downward CO₂ flux. However, others suggest that, due to poleward intensified westerly winds in the Southern Ocean, CO₂ transports in the deep ocean will increase (Russell et al. 2006; Mignone et al. 2006). Russell et al. (2006) used simulations performed until the year 2300 with two different coupled GCMs having different skills in simulating the shift of the wind fields to separate the impacts of surface warming and poleward wind intensification. They found that the shift and enhancement of the winds dominate the surface warming effect. Thus, in spite of a lower density of the surface waters, an increase of the CO₂ transports into the deep ocean would occur owing to a robust overturning in the Southern Ocean due to enhanced wind fields. The coupled simulation of our study also shows an enhancement and southward shift of the wind stress belt, leading to an increased gas transfer velocity and, together with sea ice melting in the polar areas, to a considerable net CO₂ flux into the ocean (Fig. 13). This effect is however exceeded by partial pressure difference and solubility effects. Hence, in our coupled simulation the Southern Ocean reduces CO₂ uptake compared with the fixed climate simulation. The strong increase of CO₂ uptake in the Southern Ocean and adjacent seas that we found in both, the coupled and the uncoupled simulation is due to the increased emissions, i.e. atmospheric CO₂ concentrations, and not to the modifications of the wind stress fields. This is in contrast to Russell et al. (2006), who, and this should be kept in mind, exploited the last centuries of the twenty-third century, when there is a strong increase of the ACC. We exploit the last decades of the twenty-first century, when there is still no evidence for an increase of the ACC in the coupled simulation to that time.

The second largest response of atmosphere/ocean CO₂ flux to climate change is found in the North Atlantic, which is even larger by unit area than in the Southern Ocean (Fig. 3). This is in line with Sarmiento et al. (1998) and Maier-Reimer et al. (1996), who also attributed the climate change induced CO₂ uptake reduction in the North Atlantic to the decrease of the North Atlantic MOC. Matear and Hirst (1999) found a reduction of anthropogenic CO₂ flux into the ocean as a consequence of a decrease of MOC, convective mixing and increased stratification in the high latitudes followed by climate change. They investigated a set of simulations of a

coupled atmosphere–ocean model—with no land module included—forced by IS92a and separated the effects of changing ocean circulation, increasing SST and CO₂ emissions to the oceanic CO₂ uptake. At the end of the twenty-first century, the circulation and the surface warming effects on the oceanic response to CO₂ flux changes have similar magnitudes. In contrast, in our simulations a dominant response of partial pressure difference in the North Atlantic is obtained, reflecting the dominant role of reduced MLD and MOC.

In the Southern Ocean south of 60° S (except the Weddell Sea) and in the Arctic Ocean, we find an enhancement of CO₂ uptake, i.e. a negative feedback that masks the positive feedback by around 20%. These increases are a consequence of sea ice melting, enhancing both the gas transfer and the biological production. Sea ice melting is commonly assumed to occur and simulated under global warming (Lefebvre and Goosse 2007a, b), however, the effect of sea ice melting to the CO₂ flux into the ocean has not been quantified before. CO₂ flux change contributions from additional sea ice melting only occur as long as sea ice exists. When continuous atmospheric warming further on leads to sea ice melting, the direct air–sea interface finally reaches its maximum extent. Furthermore, in our simulation export is limited due to the limited light supply for photosynthesis in high latitudes, inhibiting large export contributions. Therefore, the partial compensation of the slowdown of ocean CO₂ uptake by sea ice melting is limited and leads only to a temporal shift of the ocean's response to climate change, masking the decreases due to changes of solubility and partial pressure difference. Thus, an acceleration of the CO₂ uptake reduction accompanied with climate change is expected when sea ice will have disappeared.

In the low latitudes, except in the Atlantic, the response of oceanic CO₂ uptake is negligible. Here, different processes compensate each other. For example, in the eastern Equatorial Pacific reduced out-gassing due to increased stratification and consequently less upwelling of CO₂-rich water masses obviously cancels the reduced CO₂ uptake due to reduced export, which is accompanied by reduced upwelling of nutrient-rich waters. Cox et al. (2000) also found that reduced biological production due to reduced upwelling actually occurs, but is offset by the weaker upwelling of carbon-enriched water from deeper layers. On the whole, changes of biology are mainly confined to the low latitudes and those polar areas where sea ice melting leads to increasing insolation. In the Southern Ocean (between 30° and 60°S) and its northern adjacent seas, which represent a dominant future CO₂ sink, the climate change effect on biology remains small. This is suggested to be a consequence of iron-limitation, which is especially

effective in the Southern Ocean and leads also to small export rates in the coupled simulation. However, these results might also be model-dependent. Given the large uncertainties in the oceanic biological parameterizations, this needs further exploitation. Bopp et al. (2005) examined a climate model coupled with ocean biogeochemistry of a 4 × CO₂ simulation. They found for the phytoplankton group of diatoms a reduction of up to 60% in the North Atlantic and the subantarctic Pacific. However, they also concluded that the biological processes do not dominate the response of the oceanic carbon cycle to climate change. This is also in line with e.g. Sarmiento et al. (1998), Maier-Reimer et al. (1996), Matear and Hirst (1999), Cox et al. (2000), Plattner et al. (2001), Prentice et al. (2001) and Chuck et al. (2005).

6 Conclusions

This study focuses on the properties of the atmosphere/ocean interface relevant for CO₂ fluxes. The carbon cycle of the deep ocean will be examined in a future study. From this study we draw the following conclusions:

- The oceanic CO₂ uptake continuously increases as a consequence of enhanced CO₂ emissions.
- The oceanic CO₂ uptake is weakened by climate change, on the whole representing a positive feedback with atmospheric CO₂ concentrations. This feedback is evident not until the last decades of the twenty-first century when the effect amounts to about 10% of the total air–sea CO₂ flux. This amount includes the response of the ocean to rising atmospheric CO₂ concentrations due to a more rapid terrestrial response to climate change, which partly offsets the climate change effect of the global ocean. We assume that simulations based on scenarios with a slower increase of the emissions than that used in the present study (IPCC SRES A2) yield a less rapid response of the land associated with a less increase of atmospheric CO₂ partial pressure. This would favor a more pronounced response of the ocean.
- The positive feedback of the ocean is dominated by changes of partial pressure differences, associated with changes of the maximum MLD and accompanied by a weaker MOC in the North Atlantic and less deep convection in the Southern Ocean. Solubility effects lead also to a positive feedback, which is however of secondary importance. The positive global feedback is to a large extent compensated by wind stress changes and sea ice melting, the latter inducing in the polar regions enhanced CO₂ uptake. This leads to a lagged oceanic response to climate change. When sea ice

continuously melts, this offset becomes negligible. The biological response to climate change is of secondary order.

- Our results imply that under a future reduction of CO₂ emissions and thus atmospheric CO₂ concentrations, even to present levels, the oceanic CO₂ uptake would be smaller than today's because the changed ocean circulation leads to a less-efficient oceanic CO₂ uptake than in present times.
- For a better assessment of the long-term response of the ocean's carbon cycle to anthropogenic CO₂ emissions with special emphasis on the lagged oceanic response to climate change we propose further climate projections with (a) a longer simulation time, (b) further increasing CO₂ emissions, and (c) reduced emissions aimed at a stabilization of atmospheric CO₂ concentrations.

Acknowledgments This research was financed by the European Community under the ENSEMBLES project. The simulations were performed on the NEC SX-6 supercomputer installed at the German Climate Computing Centre (DKRZ) in Hamburg. We thank the anonymous reviewers for their helpful comments.

Open Access This article is distributed under the terms of the Creative Commons Attribution Noncommercial License which permits any noncommercial use, distribution, and reproduction in any medium, provided the original author(s) and source are credited.

References

- Bengtsson L, Hodges KI, Roeckner E (2006) Storm tracks and climate change. *J Clim* 19:3518–3543
- Bopp L, O Aumont P, Cadule S, Alvain M, Gehlen (2005) Response of diatoms distribution to global warming and potential implications: a global model study. *Geophys Res Lett* 32:L19606. doi: [10.1029/2005GL023653](https://doi.org/10.1029/2005GL023653)
- Cao PM, Woodward FI (1998) Dynamic responses of terrestrial ecosystem carbon cycling to global climate change. *Nature* 393:249–252. doi: [10.1038/30460](https://doi.org/10.1038/30460)
- Chuck A, Tyrrell T, Totterdell iJ, Holligan PM (2005) The oceanic response to carbon emissions over the next century: investigation using three ocean carbon cycle models. *Tellus* 57B:70–86
- Cox PM, Betts RA, Jones CD, Spall SA, Totterdell iJ (2000) Acceleration of global warming due to carbon-cycle feedbacks in a coupled climate model. *Nature* 408:184–187. doi: [10.1038/35041539](https://doi.org/10.1038/35041539)
- Cunningham SA, SG Alderson BA, King MA, Brandon (2003) Transport and variability of the Antarctic Circumpolar Current in Drake Passage. *J Geophys Res* 108:8084. doi: [10.1029/2001JC00147](https://doi.org/10.1029/2001JC00147)
- Dufresne J-L, Friedlingstein P, Berthelot M, Bopp L, Ciais P, Fairhead L, Le Treut H, Monfray P (2002) On the magnitude of positive feedback between future climate change and the carbon cycle. *Geophys Res Lett* 29(10). doi: [10.1029/2001GL013777](https://doi.org/10.1029/2001GL013777)
- Enting I, Wigley T, Heimann M (1994) Future emissions and concentrations of carbon dioxide; key ocean/atmosphere/land analysis. Techn Pap 31, Div of Atmos Res, Commonw Sci and Ind Res Org, Melbourne

- Friedlingstein P, Bopp L, Ciais P, Dufresne J-L, Fairhead L, LeTreut H, Monfray P, Orr J (2001) Positive feedback between future climate change and the carbon cycle. *Geophys Res Lett* 28(8):1543–1546. doi:[10.1029/2000GL012015](https://doi.org/10.1029/2000GL012015)
- Friedlingstein P, Dufresne J-L, Cox PM, Rayner P (2003) How positive is the feedback between climate change and the carbon cycle? *Tellus* 55B. doi:[10.1034/j.1600-0889.2003.01461.x](https://doi.org/10.1034/j.1600-0889.2003.01461.x)
- Friedlingstein P, Cox P, Betts R, Bopp L, von Bloh W, Brovkin V, Cadule P, Doney S, Eby S, Fung I, Bala G, John J, Jones C, Joos F, Kato T, Kawamiya M, Knorr W, Lindsay K, Matthews H, Raddatz T, Rayner P, Reick C, Roeckner E, Schnitzler K, Schnur R, Strassmann K, Weaver A, Yoshikawa C, Zeng N (2006) Climate-carbon cycle feedback analysis, results from the C4MIP model intercomparison. *J Clim* 19:3337–3353
- Fyfe JC, OA Saenko (2005) Human-induced change in the Antarctic circumpolar current. *J Clim* 18:3068–3073
- Gregory JM et al (2005) A model intercomparison of changes in the Atlantic thermohaline circulation in response to increasing atmospheric CO₂ concentration. *Geophys Res Lett* 32:L12703. doi:[10.1029/2005GL023209](https://doi.org/10.1029/2005GL023209)
- Heinze C, Hupe A, Maier-Reimer E, Dittert N, Ragueneau O (2003) Sensitivity of the marine biospheric Si cycle for biogeochemical parameter variations. *Global Biogeochem Cycles* 17:1086. doi:[10.1029/2002GB001943](https://doi.org/10.1029/2002GB001943)
- Houghton JT, Ding Y, Griggs DJ, Noguer M, van der Linden PJ, Xiaosu D (eds) (2001) Climate change 2001: the scientific basis. Contribution of Working Group I to the Third Assessment Report of the Intergovernmental Panel on Climate Change (IPCC). Cambridge University Press, Cambridge, pp 944
- Houghton RA (2003) Revised estimates of the annual net flux of carbon to the atmosphere from changes in land use and land management 1850–2000. *Tellus* 55B:378–390
- Jungclaus JH, Botzet M, Haak H, Keenylside N, Luo J-J, Latif M, Marotzke J, Mikolajewicz U, Roeckner E (2006) Ocean circulation and tropical variability in the coupled model ECHAM5/MPI-OM. *J Clim* 19:3952–3972
- Keeling CD, Whorf TP (2005) Atmospheric CO₂ records from sites in the SIO air sampling network. In: Trends: A Compendium of Data on Global Change. Carbon Dioxide Information Analysis Center, Oak Ridge National Laboratory, U.S. Department of Energy, Oak Ridge
- Key RM, Kozyr A, Sabine CL, Lee K, Wanninkhof R, Bullister JL, Feely RA, Millero FJ, Mordy C, Peng T-H (2004) A global ocean carbon climatology: results from global data analysis project (GLODAP). *Glob Biogeochem Cycle* 18:GB4031. doi:[10.1029/2004GB002247](https://doi.org/10.1029/2004GB002247)
- Knorr W (2000) Annual and interannual CO₂ exchange of the terrestrial biosphere: process based simulations and uncertainties. *Global Ecol Biogeogr* 9:225–252
- Kushner PJ, Held IM, Delworth TL (2001) Southern hemisphere atmospheric circulation response to global warming. *J Clim* 14(10):2238–2249
- Lefebvre W, Goosse H (2007a) Analysis of the projected regional sea ice changes in the Southern Ocean during the 21st century. *Clim Dyn*. doi:[10.1007/s00382-007-0273-6](https://doi.org/10.1007/s00382-007-0273-6)
- Lefebvre W, Goosse H (2007b) Analysis of the projected regional sea-ice changes in the Southern Ocean during the twenty-first century. *Clim Dyn*. doi:[10.1007/s00382-007-0273-6](https://doi.org/10.1007/s00382-007-0273-6)
- Macdonald AM (1998) The global ocean circulation: a hydrographic estimate and regional analysis. *Progress in Oceanography*, vol 41. Pergamon, New York, pp 281–382
- Maier-Reimer E, U Mikolajewicz A, Winguth (1996) Future ocean uptake of CO₂ interaction between ocean circulation and biology. *Clim Dyn* 12:711–721
- Maier-Reimer E, Kriest I, Segsneider J, Wetzel P (2005) The Hamburg Ocean Carbon Cycle Model HAMOCC5.1—Technical description release 1.1. Reports on Earth System Science 14. Available from <http://www.mpimet.mpg.de>
- Manabe S (1998) Study of global warming by GFDL climate models. *AMBIO* 27:182–186
- Marland G, Boden TA, Andres RJ (2003) Global, regional and national emissions. In: Trends: A compendium of data on global change. Carbon Dioxide Information Center, Oak Ridge National Laboratory, U. S. Department of Energy, Oak Ridge
- Marsland SJ, Haak H, Jungclaus JH, Latif M, Röske F (2003) The Max Planck Institute global ocean/sea ice model with orthogonal curvilinear coordinates. *Ocean Modelling* 5:91–127
- Matear RJ, Hirst AC (1999) Climate change feedback on the future oceanic CO₂ uptake. *Tellus* 51B:722–733
- McNeil BI, Matear RJ, Key RM, Bullister JL, Sarmiento JL (2003) Anthropogenic CO₂ uptake by the ocean based on the global chlorofluorocarbon data set. *Science* 299:235–239
- Mignone BK, Gnanadesikan A, Sarmiento JL, Slater RD (2006) Central role of Southern Hemisphere winds and eddies in modulating the oceanic uptake of anthropogenic carbon. *Geophys Res Lett* 33:L01604. doi:[10.1029/2005GL024464](https://doi.org/10.1029/2005GL024464)
- Murnane RJ, Sarmiento JL, Le Quééré C (1999) Spatial distribution of air-sea CO₂ fluxes and the interhemispheric transport of carbon by the oceans. *Glob Biogeochem Cycl* 13(2):287. doi:[10.1029/1998GB900009](https://doi.org/10.1029/1998GB900009)
- Plattner GK, Joos F, Stocker TF, Marchal O (2001) Feedback mechanisms and sensitivities of ocean carbon uptake under global warming. *Tellus* B 53(5):564–592. doi:[10.1034/j.1600-0889.2001.530504.x](https://doi.org/10.1034/j.1600-0889.2001.530504.x)
- Prentice IC, Farquhar GD, Fasham MJR, Goulden ML, Heimann M et al (2001) The carbon cycle and atmospheric CO₂. In: Houghton JT, Ding Y, Griggs DJ, Noguer M, van der Linden PJ, Xiaosu D (eds) Climate change 2001: the scientific basis. Cambridge University Press, Cambridge, pp 944
- Raddatz TJ, Reick C, Knorr W, Kattge J, Roeckner E, Schnur R, Schnitzler K-G, Wetzel P, Jungclaus J (2007) Will the tropical land biosphere dominate the climate-carbon cycle feedback during the twenty-first century? *Clim Dyn*. doi:[10.1007/s00382-007-0247-8](https://doi.org/10.1007/s00382-007-0247-8)
- Roeckner E, Bäuml G, Bonaventura L, Brokopf R, Esch M, Giorgetta M, Hagemann S, Kirchner I, Kornbluh L, Manzini E, Rhodin A, Schlese U, Schulzweida U, Tompkins A (2003) The atmospheric general circulation model ECHAM 5. PART I: Model description. Max Planck Institute for Meteorology, Report 349
- Roeckner E, Stier P, Feichter J, Kloster S, Esch M, Fischer-Bruns I (2006) Impact of carbonaceous aerosol emissions on regional climate change. *Clim Dyn*. doi:[10.1007/s00382-006-0147-3](https://doi.org/10.1007/s00382-006-0147-3)
- Russell JL, Dixon KW, Gnanadesikan A, Stouffer RJ, Toggweiler JR (2006) The Southern Hemisphere Westerlies in a warming world: propping open the door to the deep ocean. *J Clim* 19(24):6382–6390
- Sabine CL, Feely RA, Gruber N, Key RM, Lee K, Bullister JL, Wanninkhof R, Wong CS, Wallace DWR, Tilbrook B, Millero FJ, Peng T-H, Kozyr A, Ono T, Rios AF (2004) The oceanic sink for anthropogenic CO₂. *Science* 305:367–371
- Sarmiento JL (1992) Biogeochemical ocean models. In: Trenberth K (ed) Climate systems modeling. Cambridge University Press, Cambridge, pp 519–551
- Sarmiento JL, Hughes TMC, Stouffer RJ, Manabe S (1998) Simulated response of the ocean carbon cycle to anthropogenic climate warming. *Nature* 393:245–249
- Sarmiento JL, Hughes TMC (1999) Anthropogenic CO₂ uptake in a warming ocean. *Tellus* 51B:560–561
- Sarmiento JL, Gruber N (2002) Sinks for anthropogenic carbon. *Phys Today* 55(8):30–36
- Sarmiento JL, Slater R, Barber R, Bopp L, Doney SC, Hirst AC, Kleypas J, Matear R, Mikolajewicz U, Monfray P, Soldatov V,

- Spall SA, Stouffer R (2004) Response of ocean ecosystems to climate warming. *Global Biogeochem Cycles* 18:GB3003. doi:[10.1029/2003GB002134](https://doi.org/10.1029/2003GB002134)
- Stouffer RJ, Yin J, Gregory JM, Dixon KW, Spelman JM, Hurlin W, Weaver AJ, Eby M, Flato GM, Hasumi H, Hu A, Jungclaus JH, Kamenkovich IV, Levermann A, Montoya M, Murakami S, Nawrath S, Oka A, Peltier WR, Robitaille DY, Sokolov A, Vettoretti G, Weber SL (2006) Investigating the causes of the response of the thermohaline circulation to past and future climate changes. *J Clim* 19(8):1365–1387
- Takahashi T, Sutherland SC, Sweeney C, Poisson A, Metzler N, Tilbrook B, Bates N, Wanninkhof R, Feely RA, Sabine C et al (2002) Global sea-air CO₂ flux based on climatological surface ocean pCO₂, and seasonal biological and temperature effects. *Deep-Sea Res II* 49:1601–1622
- Timmreck C, Schulz M (2004) Significant dust simulation differences in nudged and climatological operation mode of the AGCM ECHAM. *J Geophys Res* 109:D13202. doi:[10.1029/2003JD004381](https://doi.org/10.1029/2003JD004381)
- Valcke S, Caubel A, Declat D, Terray L (2003) OASIS ocean atmosphere sea ice soil user's guide. Technical Report, TR/CMGC/03/69, CERFACS, Toulouse
- Weiss RF (1970) The solubility of nitrogen, oxygen and argon in water and sea water. *Deep-Sea Res* 17:721–735
- Weiss RF (1974) Carbon dioxide in water and sea water: The solubility of a non-ideal gas. *Mar Chem* 2:203–215
- Wetzel P, Winguth A, Maier-Reimer E (2005) Sea-to-air CO₂ flux from 1948 to 2003: A model study. *Glob Biogeochem Cycl* 19:GB2005. doi:[10.1029/2004GB002339](https://doi.org/10.1029/2004GB002339)
- Wunsch C (2002) What is the thermohaline circulation? *Science* 298:1179–1180
- Yin JH (2005) A consistent poleward shift of the storm tracks in simulations of 21st Century climate. *Geophys Res Lett* 32:L18701. doi:[10.1029/2005GL023684](https://doi.org/10.1029/2005GL023684)